JOURNAL OF Materials CHEMISTRY

# Tin sulfide clusters in zeolite Y, $Sn_4S_6$-Y

**Carol L. Bowes and Geoffrey A. Ozin***

*Materials Chemistry Research Group, Lash Miller Chemical Laboratories, University of Toronto, 80 St. George St., Toronto, Canada, M5S 3H6*

The synthesis of a tin sulfide cluster array, denoted $Sn_4S_6$-Y, using the quantitative sequential surface anchoring and reaction of tetramethyltin with hydrogen sulfide (metal organic chemical vapor deposition, MOCVD, reagents) within the supercages of acid zeolite-Y is detailed. The tethered methyltin species and their transformation to the encapsulated tin sulfide clusters are elucidated through gravimetry, coupled with mid-IR and $^{119}$Sn Mössbauer spectroscopy. Transmission electron microscopy (TEM) and Rietveld refinement of synchrotron powder X-ray diffraction (PXRD) data show that the clusters are internally confined and homogeneously dispersed in the supercages of the host zeolite, while optical spectroscopy show a cluster size dependent blue-shift of the absorption edge with respect to the bulk tin sulfide phase. A geometry is proposed for the encapusulated $Sn_4S_6$-Y cluster.

## Introduction

Various approaches to the fabrication of semiconductor quantum dots have been explored, both 'top-down' and 'bottom-up'.[1] The former starts with two-dimensional quantum well structures formed usually by molecular beam epitaxy or chemical vapour deposition, followed by lithography, etching and milling techniques to reduce the lateral dimensions and form cylindrical dots.[2] Great gains have been made in recent years and the minimum size of such structures has decreased. Dots on the order of tens of nanometers can be created using modified STM, but not on a practical production scale, and by sub-optical lithography, although the thicknesses of dots made using this technique tend to be many times this size.[3] Variations of this form of fabrication include the construction of nanoelectrodes within the quantum well structure so that electric fields can be produced to 'squeeze' the electrons and holes electrostatically.[4] In this way coupling between the dots can be controlled and adjusted *via* an applied gate-voltage. Structures have been made in which layers are created 'epitaxially' such that they are not well lattice-matched, resulting in a strained interface. Selective etching of the straining layer relieves the compressive stress locally and results in confinement of the charge carriers in that area.[5]

The 'bottom-up' route involves chemical synthesis in which attempts are made to tailor the size, shape and distribution of semiconductor nanoclusters using self-limiting techniques.[6] This was initially approached by solution-phase synthesis with organic capping[7] or through sol–gel-type synthesis.[8] Alternatively, synthesis within structured media was employed to constrain size. This was originally attempted in micelles, vesicles and lipid bilayers, polymers, glasses, clays, and zeolites.[9–12] Organic-passivated clusters are now prepared in macroscopic quantities with tunable sizes of 15–100 Å with a standard deviation of less than 4%, and can be manipulated to form superlattices of close-packed nanoclusters as faceted crystals or thin films.[13] Colloidal chemistry is used to produce layered nanocrystals, for example CdS/HgS/CdS, with epitaxial matching between the core and layers.[14] It has also been found that nanoclusters will self-assemble at high-strain regions when direct epitaxy is performed on the slopes of the valleys of a corrugated layer. Such nanoclusters even self-align to form quasi-ordered arrays.[15]

In this paper a self-limiting synthetic approach is described which takes advantage of the host–guest chemistry of acid zeolite Y, in which the quantitative sequential anchoring and reaction of tetramethyltin with hydrogen sulfide forms tin sulfide clusters within the zeolite supercages.

## Experimental

### Materials

Acid zeolite Y was prepared by repeated ion-exchange of calcined and defect-removed $Na_{56}Y$ (UOP Y-52 lot no. 13076-81) with ammonium nitrate. Crystallinity was confirmed by powder XRD; $^{27}$Al MAS NMR indicated no occluded aluminous material and $^{29}$Si MAS NMR confirmed the Si/Al ratio.[16] Dehydrating at 430 °C resulted in deammination, leaving protons as charge-balancing cations. At this stage, the resulting material was very moisture sensitive, and was maintained under high vacuum ($10^{-5}$ Torr) for subsequent steps. Elemental analysis (Galbraith, ICP) indicated a unit cell formula of $H_{44}Na_{12}[(AlO_2)_{56}(SiO_2)_{136}]$ corresponding on average to 5.5 protons and 1.5 $Na^+$ ions per α-cage and β-cage. Tetramethyltin (Aldrich, 99 + %) was stored over a molecular sieve and degassed by a freeze–evacuate–thaw cycle. $H_2S$ (Matheson, 99.5%) was passed through freshly dehydrated sodium Y zeolite before use.

### Synthetic methods

Most reactions involving the zeolite were carried out on a self-supporting pressed disk of acid zeolite Y (approximately 40 mg) in an *in situ* cell which allowed dehydration, incremental $Me_4Sn$ adsorption, and had NaCl and quartz windows to allow mid-IR and UV–VIS spectroscopy.[17] Some experiments were performed in a small reaction cell on larger amounts of acid zeolite Y to allow gravimetric measurements. In general, the cluster was produced by dehydrating and deaminating the zeolite wafer at 430 °C, followed by cooling under dynamic vacuum. Degassed tetramethyltin was introduced incrementally by allowing the vapour above the liquid to expand into a small 'titration' volume and then allowing this volume of gas to enter the main body of the closed *in situ* cell. After allowing the gas to adsorb into and react with the zeolite for a brief time (*ca.* 15 min), the wafer was heated in the quartz end of the sample cell to 150 °C for 2 h, after which it remained white. The sample cell was then returned to the vacuum line, evacuated and filled to 150 Torr with dry $H_2S$. The wafer was again heated for 2 h at 150 °C, whereupon it turned a pale golden yellow colour, and the cell was evacuated. Any further handling of the sample was performed under inert atmosphere.

### Characterization

FT-mid-IR spectra were collected on a Nicolet 20SXB (resolution 2 $cm^{-1}$) by co-adding 100 interferograms. UV–VIS

diffuse reflectance spectra were recorded with respect to $BaSO_4$ standards on a Perkin-Elmer 330 spectrophotometer using an integrating sphere attachment. Data were digitized and converted to absorbance using Kubelka–Munk theory.[18] Powder X-ray diffraction data collected for Rietveld structure refinement were obtained at Brookhaven National Laboratories on beam-line X7A of the synchrotron. A germanium double crystal monochromator was used to select wavelengths of about 0.7 Å, which was detected by a Kevex solid-state detector. Samples were sealed in Lindemann capillary tubes, cooled to 15 K, and rocked by about 2° while data were collected in 0.005° intervals between 2 and 50° $2\theta$, with collection times increasing with increasing $2\theta$ for a total of 12 h. Data were analyzed using GSAS software.[19] $^{119}$Sn Mössbauer data were collected in constant acceleration mode using a Ranger Scientific MS-1200 instrument. The radiation source was 5 mCi $^{119}$Sn in a $CaSnO_3$ matrix. Data were collected at room temperature or at 77 K relative to $SnO_2$. Semi-quantitative (2.5 atom%) scanning electron microscopy with energy dispersive X-ray microanalysis, SEM–EDX, was performed by Imagetek, using a Hitachi 800 analytical transmission electron microscope operating at 100 kV. The probe size was 50 nm in area and penetrated greater than 1 μm in depth. A LINK X-ray microanalyser was employed for data analysis, and SnS and $SnS_2$ were used as standards. Independent elemental analysis was performed by Galbraith Laboratories, Inc., using ICP for Si, Al, and Sn determinations and for C, the IR intensity of CO resulting from sample combustion. TEM images of the lattice at more than $1.2 \times 10^6$ times magnification were obtained also by Imagetek using a Hitachi 7000 transmission electron microscope, operating at an accelerating voltage of 100 kV. The resolution was estimated conservatively at 4.5 Å. Exposure times were limited to 2 s as electron beam induced sample alteration was observed at times of 45 s or more. Extended Hückel molecular orbital, EHMO, calculations were undertaken for isolated tin sulfide clusters, $Sn_4S_6$, using the ICONCL software.[20] The program used the standard EHMO theory wherein atomic ionization potentials were used for $H_{ii}$ and $H_{jj}$, and $H_{ij}$s were calculated using the Wolfsberg–Helmholtz approximation, $H_{ij}=1/2K(H_{ii}+H_{jj})S_{ij}$. Overlap integrals, $S_{ij}$, were calculated for all atomic orbitals rather than just nearest neighbours, using Slater-type orbitals. A weighted Wolfsberg–Helmholtz approximation, $K=k'+\Delta^2+\Delta^4(1-k')$ where $\Delta=(H_{ii}-H_{jj})/(H_{ii}+H_{jj})$ and $k'$ is a constant,[21] was used in this program to account for the differing 'diffuseness' characteristic of complexes containing unoccupied high-energy basis functions. In addition, a distance dependence for $K$ was included, according to the work of Calzaferri *et al.*[22]

## Results and Discussion

The internal surface of acid zeolite Y is ideal for MOCVD because the protons, which are charge balancing in the structure, can participate in surface anchoring thereby providing control over reaction stoichiometry. The reaction and regeneration of protons as well as their solvation and migration are all observable by mid-IR spectroscopy. Thus the progress of the host–guest chemistry can be monitored *in situ* providing control over the cluster assembly process.[23]

### Synthesis details

**Anchoring of tetramethyltin.** Zeolite Y has an open-framework topology comprised of α- and β-cages, roughly 13 Å and 6 Å diameter, respectively, interconnected through 6 T-atom windows. In the illustration of the structure of zeolite Y shown in Fig. 1, each vertex represents a tetrahedral (T-atom) site which is either $SiO_4$ or $AlO_4^-$. Extra framework cations balance the framework charge due to the $Al^{III}$ centres, and the

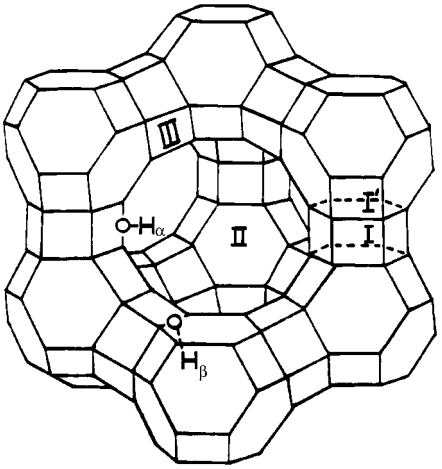


**Fig. 1** Acid zeolite Y showing 13 Å α-cage formed by 6 Å β-cages linked by double six-rings. Oxygen atoms bridge between Si and Al tetrahedral centres located at each vertex. Cation sites within the α-cage are shown, as well as Brønsted acid sites, $H_\alpha$, $H_\beta$.

specific crystallographic positions of the cations, considered oxide coordination sites in the 'zeolate' coordination chemistry model,[23,24] are indicated in Fig. 1.

The adsorption of tetramethyltin is observed in the mid-IR spectrum between 4000 and 1200 $cm^{-1}$, using an *in situ* reaction cell as described in the experimental section. Fig. 2(a) shows the spectrum of HY dehydrated at 430 °C. The bands at 3640 and 3540 $cm^{-1}$ have been assigned to the α and β bridging $\nu$OH modes.[25,26] The small peak at 3740 $cm^{-1}$ represents terminal $\nu$OH stretches, *i.e.* those OH existing on the external surface, or in hydroxyl nests and defect sites. Fig. 2(b) shows the final effect of titration of the α-proton with numerous incremental additions of thoroughly degassed tetramethyltin. The IR intensity of the α-proton was used as the indicator for the titration. The α-protons reacted, evolving methane and anchoring a trimethyltin moiety in the α-cage as follows:

$$\text{Z-O-H} + \text{Me}_4\text{Sn} \rightarrow \text{Z-O-SnMe}_3 + \text{CH}_4$$

Heating to 150 °C for 2 h resulted in the consumption of all reactive α- and β-protons, as is shown in Fig. 2(c). The resulting methane IR spectrum ($\nu_3$ and $\nu_4$ modes) was observed in the atmosphere of the sealed *in situ* cell and its intensity was measured after each step. An intensity–pressure calibration was made, in order to ensure that Beer's law holds over the pressure range studied. Acid zeolite Y is known not to adsorb methane, unlike other zeolites or other alkanes.[27,28] The further

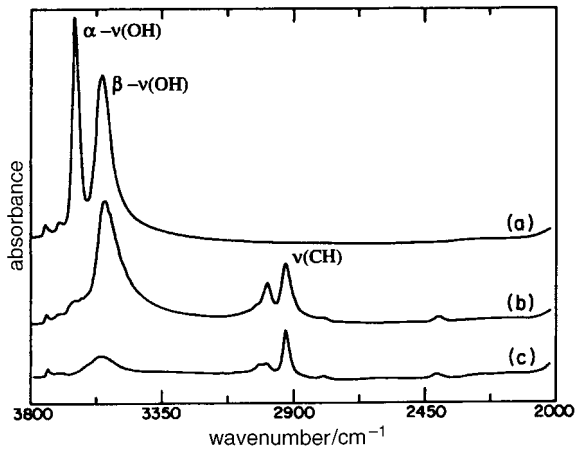


**Fig. 2** The titration of protons in zeolite Y with tetramethyltin. Mid-IR spectra of (a) dehydrated $H_{44}Na_{12}Y$, (b) spectrum following α-proton titration and tetramethyltin anchoring, (c) spectrum following reaction at 150 °C.

reaction of the anchored methyltin species with $H_2S$ (150 Torr, 150 °C, 2 h) released essentially all of the remainder of the methyl groups bound to tin as methane, the IR intensity of which was measured.

By equating the final methane intensity measured with the maximum of four methyl groups per tin, it was possible to conclude that, on average, $1.0 \pm 0.1$ methyl groups per tin were released from the titration of the four α-cage protons at room temperature, and therefore that four trimethyltin species were anchored per α-cage. By the same calculations, after reaction at 150 °C, $1.5 \pm 0.1$ methane molecules per tin were present in the atmosphere of the *in situ* cell. This corresponds to a total of 6 protons per α-cage/β-cage unit (48 per unit cell), in reasonable agreement with the 5.5 (44 per u.c.) determined by elemental analysis. After reaction at 150 °C, there is some small, remaining β-proton intensity which was thought to be either inaccessible or weakly acidic defect proton sites, lying within the β-proton bandwidth. The reaction of essentially all protons was taken to indicate the 'homogeneous dispersion' of the reactants throughout the zeolite. Although the protons are to some extent mobile, they cannot delocalize from the unit cell entirely because it would involve creating charge-separated regions in the zeolite lattice which is expected to be energetically unfavourable. Therefore, the disappearance of all protons implies the homogeneity of the anchored precursor. The reaction pathway for the tetramethyltin adsorption may be summarized as follows

$$H_{\alpha 32}H_{\beta 12}Na_{12}Y + 32Me_4Sn \xrightarrow{RT} (Me_3Sn)_{32}H_{\beta 12}Na_{12}Y + 32CH_4$$

$$(Me_3Sn)_{32}H_{\beta 12}Na_{12}Y \xrightarrow{150\,^{\circ}C} (Me_3Sn)_{20}(Me_2Sn)_{12}Na_{12}Y + 12CH_4$$

It is interesting to consider the factors contributing to the reaction path described above. One factor is the relative reactivity of the methyl groups on the tin centre. It is clear that the first methyl group reacts with a proton with ease at room temperature, while the second is less readily removed. It is expected that the nucleophilicity of the second methyl carbon will be less than that of the first because an electron releasing methyl group of $Me_4Sn$ has been replaced by an electron withdrawing oxide-type ligand of ZO-$SnMe_3$. Therefore the reactivity towards an electrophile (proton) will incrementally decrease as first, second or third methyl groups react. Also, electrostatics may contribute to the diminished reactivity. For a second methyl group to react, the proton must effectively interact with a $Me_3Sn^+$ centre bearing a formal 1+ charge. For a third, it must approach a $Me_2Sn^{2+}$ centre bearing a formal 2+ charge. Electrostatics are expected to be an important factor, based on decationization and dehydrohalogenation kinetic experiments in zeolite Y.[29] A second factor is the steric limitation imposed by the size of the α-cage. It was observed, through IR spectroscopy of the sample pellet and sample-cell atmosphere, that $Me_4Sn$ added after completion of the titration of the α-protons remained in the atmosphere of the cell (outside the zeolite), despite the presence of further unreacted β-protons. This information should be coupled with the idea that there are expected to be thermodynamic and kinetic barriers to the reaction of the β-protons. It must be so, or the initial, room temperature uptake of tetramethyltin would affect α- and β-protons equally which is not observed (RT decrease of the β-proton intensity corresponds only to 0.15 protons). Because $Me_4Sn$ is too large to enter the β-cages, the β-protons must leave the β-cage in order to react; plus, β-protons are less acidic and less mobile than their α-counterparts, as shown through adsorption and desorption energies of given bases.[30] The combination of restricted space in the α-cage and unfavourable β-proton reactivity limits the extent of $Me_4Sn$ loading at room temperature.

It is critical to this 'deductive' reaction characterization that the tin centres remain in the same oxidation state of +IV throughout. Confirmation that the anchored tin centre remained in the original oxidation state of tetramethytin was ascertained by $^{119}Sn$ Mössbauer spectroscopy, Fig. 3(a). The anchored precursor and the cluster product, which will be discussed later, have isomer shifts of 1.27 and 1.25 ($\pm 0.01$) mm $s^{-1}$, respectively. Isomer shifts of less than 1.5 define tin in oxidation state IV.[31]

**Hydrogen sulfide treatment.** After the $Me_4Sn$ reaction and anchoring were complete, the sample was subjected to approximately 150 Torr $H_2S$ at room temperature followed by 150 °C for 2 h. Fig. 4(b) displays the effect of room temperature $H_2S$ treatment, while Fig. 4(c), (d) show the results of heating at 150 °C and evacuating at room temperature, respectively. Features T, A and B are familiar; the terminal and β-proton are essentially unaffected while all remnants of the α-proton have disappeared. Vestiges of the methyl groups remain also, feature E. In experiments in which the hydrogen sulfide was introduced in small, incremental volumes, features C and D grew in together with increasing amounts of $H_2S$. Features C and D, centred at about 3000 and 2370 $cm^{-1}$, have been assigned to the solvated α-protons and its solvators, respectively: $Z-O-H_\alpha\cdots(SH_2)_n$. Earlier work[32] documented similar broad and intense peaks resulting from solvation (hydrogen bonding) of zeolite Y α-cage protons by anhydrous hydrogen halides, of which the vibration was similarly bathochromically shifted. In the earlier work, the degree of shifting of the vibration was found to depend upon the electronegativity of the halide and the number of solvating molecules. In all cases a second broad band was observed, corresponding to band D in this experiment, which also shifted with electronegativity, but to a lesser extent. It was bathochromically shifted from the expected frequency of the free molecule $\nu$HX and in this

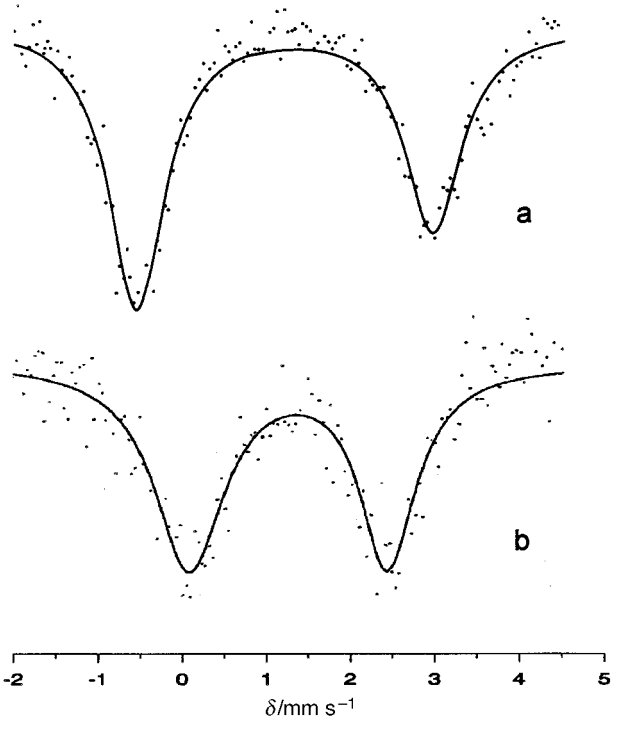


**Fig. 3** Mössbauer spectra of (a) the precursor material $(CH_3)_2Sn$-Y and (b) the product material $Sn_4S_6$-Y. Isomer shifts are reported with respect to $SnO_2$.

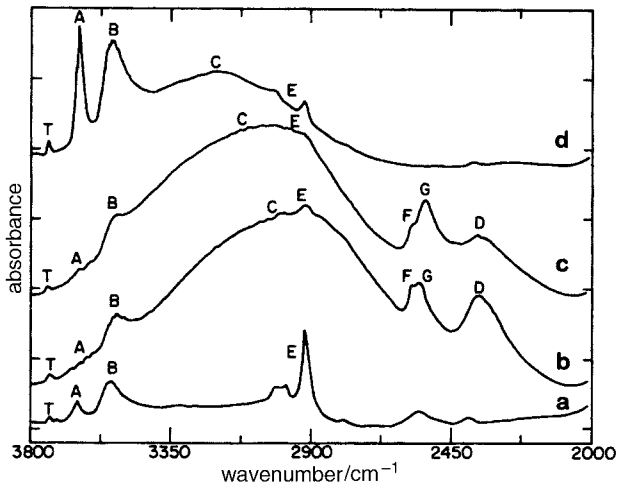


**Fig. 4** Adsorption and reaction of hydrogen sulfide in methyltin-loaded zeolite Y. (a) Mid-IR spectrum of anchored dimethyl- and trimethyltin in zeolite Y, (b) spectrum following room temperature introduction of 150 Torr $H_2S$, (c) the product of 150 °C reaction, (d) spectrum following room temperature evacuation of the reaction cell.

case the vibration may be assigned also to the *v*SH stretch for solvating hydrogen sulfide.

Finally, the peaks F and G at about 2562 cm$^{-1}$ have been assigned also to *v*SH vibrations. In the literature,[33] the $\nu_3$ mode of molecularly adsorbed hydrogen sulfide as well as the *v*SH stretching mode of a hydrosulfide group resulting from dissociatively adsorbed $H_2S$ in zeolites, have been reported at about 2560 cm$^{-1}$. While the former may be present (some $H_2S$ molecules not involved in hydrogen bonding to α-cage protons but rather physisorbed to the oxygen framework), the latter is almost certainly present, as will be considered in the discussion of the reaction path below.

Heating to 150 °C has little effect on the IR spectrum, except for a decrease in the D-band and a shift to higher frequency of the C-band, both associated with a decrease in the number of solvating $H_2S$ molecules. Also, the intensity of and ratio between bands F and G have changed, possibly indicating the reaction of, for example, $H_2S$ to form $HS^-$ species. The sample appearance, at this stage, changed from the previously white colour to a pale golden colour.

After 150 °C reaction, the excess hydrogen sulfide and methane reaction product were pumped out of the *in situ* cell at room temperature, leaving a material whose IR spectrum is shown in Fig. 4(d). The most noticeable aspect of this spectrum is that protons, both α- and β-cage, were regenerated. It is not clear at what point in the reaction scheme the protons are regenerated, because in the presence of $H_2S$ the α-protons are solvated and their number cannot be easily quantified from their IR intensity. Nevertheless, in repeated experiments, on average 40% and up to 50% of the original intensity of these bands has returned after evacuation. Band D disappeared completely, while some portion of the protons remain solvated, indicating that all of the $H_2S$ was removed but that the tin sulfide product species solvates the neighbouring protons. Finally, the bands F and G disappeared, suggesting that no hydrosulfide species remained. Reactions of the following type, in which Y represents the zeolite framework, are thought to contribute to the process observed in the IR:

hydrosulfurization–demethylation (methane evolution):

$$Me_3Sn\text{-}Y + H_2S \rightarrow Me_2(SH)Sn\text{-}Y + CH_4$$

$$Me_2Sn\text{-}Y + H_2S \rightarrow Me(SH)_2Sn\text{-}Y + CH_4$$

hydrosulfurization–deanchoring (proton regeneration):

$$Me_2Sn\text{-}Y + H_2S \rightarrow Me_2(SH)Sn\text{-}Y + H\text{-}Y$$

$$Me_2(SH)Sn\text{-}Y + H_2S \rightarrow Me_2(SH)_2Sn + H\text{-}Y$$

dehydrosulfurization–condensation (cluster assembly):

$$(SH)_4Sn + (SH)_3Sn\text{-}Y \rightarrow (SH)_3Sn\text{-}S\text{-}Sn\text{-}(SH)_2\text{-}Y + H_2S$$

The alternative reaction for the last step is an intramolecular self-dehydrosulfurization, in which a Sn=S species is formed following $H_2S$ elimination. While this step could not be ruled out *a priori*, it is not thought to contribute in light of the remainder of the data, as will be discussed. Thus the proposed synthesis in which four anchored methyltin species per α-cage are demethylated, hydrosulfurized, and self-assembled *via* dehydrosulfurization–condensation reactions accounts adequately for the formation of a tin sulfide cluster product, except for the question of cluster stoichiometry.

Several methods were employed for the determination of the tin to sulfur ratio in the nanocluster product. The first was a quantitative gravimetric experiment in which the entire synthesis was carried out on a large sample (approximately 300 mg) in a small cell (approximately 60 g) which was accurately weighed after each step in the reaction process. The second was semiquantitative SEM–EDX using SnS and $SnS_2$ standards. A conservative estimate of the error is $\pm 2.5$ atom% for ratio measurements with standards and within the thin crystal limit for micro-X-ray fluorescence.[34] The third was independent elemental analysis (Galbraith) using ICP and with standards to establish errors. The results were as follows:

gravimetric: $S/Sn = 1.63 \pm 0.05$
STEM–EDX: $S/Sn = 1.42 \pm 0.04$
Galbraith: $S/Sn = 1.50 \pm 0.15$

giving an average result of 1.5 for the S/Sn ratio and therefore a likely cluster stoichiometry of $Sn_4S_6$, with an overall charge of 4+ based on $Sn^{IV}$ and $S^{-II}$ oxidation states, Fig. 3(b), see Mössbauer discussion above.

The absence of any significant contribution from tin sulfide material aggregating on the external surface of the zeolite crystals was determined by TEM lattice imaging, Fig. 5. Aggregations of the heavier guest species generally appear as darker spots on the crystal surface which was not observed in any TEM images obtained from many of these materials. In addition, a general impression of the homogeneity of the interior structure can be obtained which suggests that the tin sulfide clusters are encapsulated and homogeneously distributed. In fact, because not all protons are regenerated in the tin sulfide cluster formation process, it is expected that the clusters are anchored to the lattice, performing some framework charge-balancing function, in accord with the expected charge on $Sn_4S_6^{4+}$.

Finally, the regeneration of unsolvated protons has important ramifications with respect to cluster growth within the zeolite. Preliminary molecular graphics structural models indicated that a $Sn_4S_6$ cluster would not fill the α-cage void space and this idea is supported in that there exist α-protons unsolvated by the cluster in the final product. In principle, it should be possible to re-titrate the regenerated protons and in a second, controlled loading step add tin and sulfur to the existing clusters in order to increase their size. Doping might also be achieved in this way.

Growing the clusters was accomplished as shown in Fig. 6, where each IR spectrum represents a complete $Me_4Sn$ titration and anchoring/$H_2S$ adsorption and reaction/evacuation cycle. Important aspects of these spectra are the decrease of both solvated and unsolvated protons and the lack of increase of methyl or hydrosulfide group intensity. The former indicated that more of the cation sites are occupied 'capping' the clusters, the latter suggests that methyl groups are decreasingly required

**Fig. 5** Typical high resolution TEM lattice image at $1.2 \times 10^6$ magnification of zeolite Y with encapsulated tin sulfide clusters, showing lack of external tin sulfide and homogeneity of sample

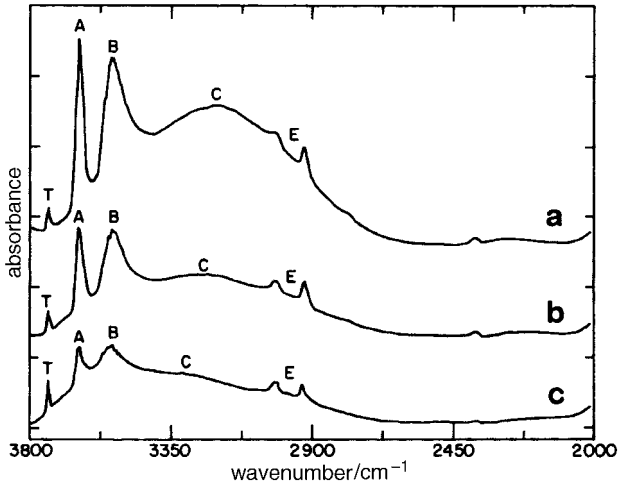


**Fig. 6** Mid-IR spectra of (a) $Sn_4S_6$ clusters in zeolite Y, (b) product following a second loading of tetramethyltin and hydrogen sulfide, and (c) following third loading

to satisfy tin coordination sites and that hydrosulfide condensation is occurring. Possibly, the new material is incorporated to form larger clusters rather that forming new, smaller clusters which would leave many tin atoms coordinatively unsaturated. Using the methods of methane quantification described earlier, the reactions of second and third $Me_4Sn$ loadings were shown to produce as much as 118% as much methane as the first, suggesting eight Sn atoms or more per α-cage. The UV–VIS spectra of the materials illustrate the cluster generation and growth nicely, and are discussed in a later section.

**Reaction pathway.** Although the reactions presented above are thought to represent those participating in cluster formation, it is the step-wise nature of this process which is perhaps most significant. Having control over the process, the ability to stop, and change the reaction conditions at any point in the synthesis is what is most unusual, and most useful about this method. Therefore it is interesting to consider what species are present at various points; in short, to consider the reaction pathway. The reaction of methyltin moieties with protons is fairly straightforward, as was described above, the first loss of methane occurring easily at room temperature, and the second with a higher activation energy due to the change in nucleophilicity and electrostatics. Thus the anchoring of $Me_4Sn$ in HY finished with a mixture of anchored trimethyl- and dimethyltin, there being 5.5–6.0 reactive protons and 4 tin centres per α-cage.

At room temperature, upon $H_2S$ addition, methane is released corresponding to almost one equivalent per tin ($0.85 \pm 0.10$) so that $2.4 \pm 0.1$ of the four methyls per tin have been released. This is curious, since the reacting species were mixed di- and trimethyltin species. No argument based on relative Sn—C bond strengths will easily account for this observation. The outcome of the reaction must depend upon which other factor was dominant. First, the degree to which the H—S bond of coordinating $H_2S$ is polarized by the tin centre will affect the reactivity of the proton. The replacement of methyl groups by hydrosulfide groups would increase the ability of tin to polarize that bond. Second, the susceptibility of the methyl carbon to electrophilic attack will be decreased by the introduction of hydrosulfide groups about the tin centre that are more electron withdrawing, having the effect of attracting electron density away from carbon and decreasing its nucleophilicity.

If the reactivity of the $H_2S$ proton were the limiting step, tin nuclei with fewer electron donating methyl groups and more electron withdrawing hydrosulfide groups would be more reactive. After a dimethyltin species reacted, it would become even more reactive, and one equivalent of methane could result from those centres alone. Alternatively, if the reactivity of the carbon were limiting, then the result might be that a centre, having gained one hydrosulfide group, would be invulnerable to further attack at room temperature, so that methane produced represents one methane from each centre. Neither scheme accounts for interference by de-anchoring proton regeneration reactions which may compete for hydrogen sulfide protons. Described in reaction (2) above, the dissociative de-anchoring must occur in order to form a tin sulfide cluster. The IR band corresponding to solvated protons in Fig. 4(a) seems too large to be entirely due to a few 'leftover' protons, yet it is not possible to quantify the amount, as the intensity is dependant both on the number of solvated protons and on their extent of solvation, as described above. However, it is likely that there is a sufficiently large excess of hydrogen sulfide so that the methane production and de-anchoring can proceed without mutual interference.

The second process is that of cluster formation self-assembly, described in reaction (3). After thermal treatment, Fig. 4(c), a strong *ν*SH vibration remained (feature G), along with some significant number of solvated protons (C). This is taken to indicate that many, if not all, species are in the hydrosulfide form, and only condense and assemble when the excess hydrogen sulfide is pumped from the cell.

**Proposed cluster geometry of $Sn_4S_6$-Y.** There exist in the literature a number of tin sulfide clusters of various stoichiometries and cluster charges having specific geometries.[35] However, the clean chemistry leading to the cluster and various pieces of evidence have led us to propose a single $Sn_4S_6$ cluster moiety. Firstly, the only example of a cluster of this stoichiometry in the literature is the recurring adamantanoid geometry with a 4+ charge. Because the clusters in the zeolite are partially charge balancing with respect to the anionic framework, creating larger clusters would involve separation

of charge between the anionic lattice and cationic clusters which would be energetically unfavourable. Further evidence was obtained from a Rietveld refinement of the structural model. Rietveld PXRD refinement is the most widely used method for obtaining crystal structures of materials when it is not possible to obtain crystals of sufficient size for single crystal structure determination, provided a good starting model is available. In the case of tin sulfide in zeolite Y the quality of the refinement was insufficient to completely define the cluster, due to significant symmetry-related disorder intrinsic in the problem, and possibly dynamic disorder, therefore the information gleaned must be taken cautiously due to the known pitfalls of locating extraframework species in zeolites.[36] Nevertheless some further evidence for its structure and location was suggested. Using the low temperature (15 K) synchrotron PXRD data, a preliminary Rietveld structure refinement of the zeolite framework only was made in the space group $Fd\bar{3}m$, in order to locate electron density on a Fourier difference map. All electron density was located in the α-cage, the β-cage being completely empty, as was expected due to the size of the precursor species. This confirms the 'α-cage specific' nature of this kind of intrazeolite MOCVD synthesis. The most significant concentration of electron density was located over the site II positions (see Fig. 1), centred above the three prominent oxygens of the six-ring in the α-cavity, at a distance of about 2.4 Å. Introducing a tin atom at this location significantly reduced the refinement residuals and $\chi^2$. The occupancy of this site, determined to be slightly less than one quarter, is indicative of a single species symmetry disordered over the four crystallographically inequivalent sites, rather than multiple species each occupying one of the sites which would lead to occupancies of one half or higher. No significant electron density was observed at any of the other common cation sites of the α-cages of zeolite Y. It was possible to introduce a second distinct tin at a location of high electron density which, due to the threefold symmetry of the site, formed a tetrahedron with the first with tin–tin distances of approximately 3.5 Å, consistent with the sulfur-bridged tins of the proposed adamantanoid geometry. This also resulted in significant reduction in residuals. Beyond this point, at which $\chi^2=2.4$, $R_p=9.1$ and weighted residual $wR_p=12.6$ (Table 1), no further improvement in the refinement could be made, despite the observation of electron density on the Fourier difference map at locations suitable for sulfur positions. Consequently, no sulfur atoms are included in the model. Although the Rietveld refinement of the data was not able to unambiguously define the structure of the tin sulfide cluster, the information that was obtained was consistent with the proposed adamantane geometry and location exclusively inside the zeolite α-cages.

**Table 1** Atom positions and parameters of the best model for a single $Sn_4S_6^{4+}$ cluster in zeolite Y

| | *x* | *y* | *z* | $U_{iso}$/Å$^2$ |
|---|---|---|---|---|
| Si/Al(1/2) | −0.0549(3) | 0.1328(2) | 0.0356(3) | 0.0039 |
| O(3) | 0 | 0.1111(6) | −0.1111(6) | 0.0366 |
| O(4) | −0.0023(5) | −0.0023(5) | 0.1459(6) | 0.0050 |
| O(5) | 0.0752(4) | 0.0752(4) | −0.0317(7) | 0.0176 |
| O(6) | 0.0713(6) | 0.0713(6) | 0.3224(8) | 0.0068 |
| Sn(7) | 0.2421(7) | 0.2421(7) | 0.2421(7) | 0.1377 |
| Sn(8) | 0.411(13) | 0.411(13) | 0.205(15) | 0.1292 |
| statistics of refinement | | $\chi^2=2.4$ | $wR_p=12.6$ | $R_p=9.1$ |
| lattice parameter, *a*/Å | | 24.6537(5) | | |
| *r*[Sn(7)−O(4)]/Å | | 2.398(20) | | |
| *r*[Sn(7)−Sn(8)]/Å | | 3.5(3) | | |
| *r*[Sn(8)−Sn(8)]/Å | | 4.7(8) | | |
| [Sn(8)−Sn(7)−Sn(8)]/° | | 83(6) | | |
| [O(4)−Sn(7)−O(4)]/° | | 101.3(9) | | |

## Spectroscopic characterization of precursors and products

**IR Spectroscopy of anchored methyltin reagents in zeolite Y.** A key tool in determining the product of the first step anchoring reaction has been *in situ* mid-IR spectroscopy. Yet, it was not possible to identify the products directly from their spectra, both because of the occurrence of mixed species, and because the spectra of the various candidates are quite similar. Fig. 7 shows the spectra in question. Trace (a) is the *ν*CH stretching region of $Me_4Sn$ chemisorbed in $Na_{56}Y$, any excess physisorbed $Me_4Sn$ having been pumped away. This represents a saturation loading of four $Me_4Sn$ per α-cage, in which the $Me_4Sn$ moieties are most likely adsorbed to the $Na^+$ cations with interactions between the methyl hydrogens and the oxygen framework sites. Trace (b) of Fig. 7 is the *ν*CH IR spectrum of the corresponding situation in HY whereby trimethyltin acts as an extraframework cation, probably situated above the four tetrahedrally arranged, puckered oxygen six-ring sites, with up to three of the adjacent oxygens coordinating the tin centre. Trace (c) of Fig. 7 is the corresponding *ν*CH IR spectrum of the product of thermal treatment of the sample in (b), expected to be roughly a 50–50 mixture of trimethyltin and dimethyltin anchored species (due to 5.5–6 total protons reacting with 4 tetramethyltin species).

Tetramethyltin is a regular tetrahedral molecule belonging to the point group $T_d$. The set of twelve displacement vectors representing the C—H stretches generate an irreducible representation $\Gamma_{vib}=A_1+E+T_1+2T_2$. Of these, only the $T_2$ are IR active. The predicted two major $T_2$ *ν*CH bands of $Me_4Sn$ in NaY were observed at 2975 and 2902 cm$^{-1}$. These values correspond to the reported $\nu_{asym}$ and $\nu_{sym}$ modes of liquid $Me_4Sn$ observed at 2982 and 2914 cm$^{-1}$ respectively.[37] In that work it was assumed that the vibrational coupling between the *ν*CH methyl group and Sn—C skeletal modes was small. On the basis of this argument, it might be expected that the difference in *ν*CH vibrational frequencies between $Me_4Sn$, $Me_3Sn$ and $Me_2Sn$ species anchored in the α-cage of zeolite Y should be small. This is the case in practice.

The nine internal coordinates representing C—H stretches for a $C_{3v}$ pyramidal, anchored ZO-Sn$(CH_3)_3$ moiety generate an irreducible representation $\Gamma_{vib}=2A_1+A_2+3E$. Of these $A_1$

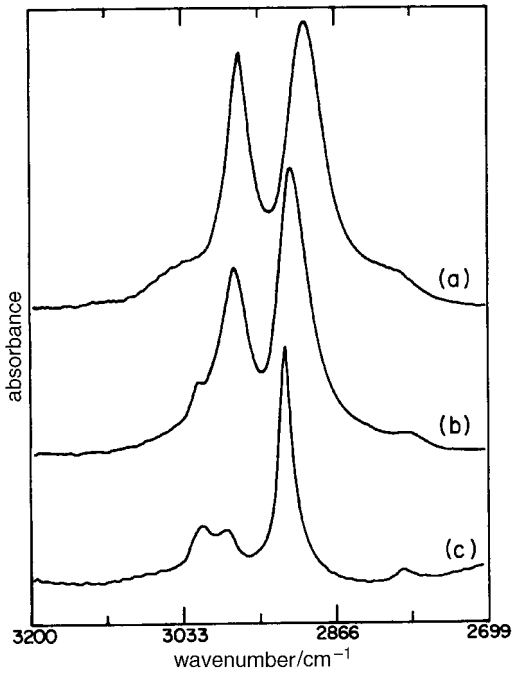


**Fig. 7** Mid-IR spectra of *ν*CH region for (a) tetramethyltin impregnated NaY, (b) anchored trimethyltin in acid zeolite Y, (c) anchored dimethyltin and trimethyltin in acid zeolite Y

and E are IR active and so five modes are expected. The two major bands observed are blue-shifted from those of chemisorbed $(CH_3)_4Sn\cdots NaY$ by roughly 15 $cm^{-1}$ for the symmetric stretch and 4 $cm^{-1}$ for the asymmetric stretch. These *v*CH bands, however, remain within the linewidths of the tetramethyltin vibrations. It is possible, through consideration of the characteristic motions which compose the *v*CH normal modes of ZO-$Sn(CH_3)_3$, to separate the five normal *v*CH modes into two sets having their origins in the symmetric and asymmetric *v*CH modes of uncoupled $CH_3$ groups. The result is that the lower frequency band may be assigned as $A_1+E$ ($A_1$, $CH_3$), while the higher frequency major band includes the components $A_1+2E$ (E, $CH_3$), the $A_2$ contribution being IR inactive.

Upon heating the ZO-$Sn(CH_3)_3$ samples containing β-protons to 150 °C, for 2 h, some ZO-$Sn(CH_3)_2$ species are formed. The spectrum shows a further shift of the band maxima to higher frequency, and a change in the relative intensities. The lower frequency band shifts by 3 $cm^{-1}$ and the higher by 5 $cm^{-1}$ with respect to the anchored ZO-$Sn(CH_3)_3$ species. As above, under $C_{2v}$, the irreducible representation $\Gamma_{vib}=2A_1+A_2+2B_1+B_2$ can be split into two groups, $A_1+B_1$ ($A_1$, $CH_3$) for the lower frequency band and $A_1+B_1+B_2$ (E, $CH_3$) for the higher frequency band.

In these considerations, a rigid model for the methyl groups has been assumed. While it is also possible to predict the active modes using a non-rigid Bunker-type model in which the methyl groups are free to rotate, in the sterically hindered environment of the α-cage containing a total of four ZO-$Sn(CH_3)_3$ and ZO-$Sn(CH_3)_2$ species, it is unlikely the methyl groups would truly be free rotors, and therefore the rigid oscillator approach was preferred. There are very weak satellite bands or shoulders in the *v*CH spectra which are, in every case, split off from the major bands by about 35 to 130 $cm^{-1}$, precluding the simple assignment of these bands as components of the *v*CH ZO-$Sn(CH_3)_3$/ZO-$Sn(CH_3)_2$ modes.[38] Such splittings are not readily accounted for through arguments of multiple anchoring site effects, splitting of degeneracy through site symmetry effects, or even correlation coupling effects, which are all typically 20 $cm^{-1}$ or less. No Raman modes of $Me_4Sn$ occur at appropriate frequencies such that a change of selection rules due to site symmetry effects could result in IR-active modes at these positions. The best interpretation is that these shoulders and weak bands be assigned as overtones and combinations with low frequency fundamental modes, consistent with the assignment of similar shoulders in the spectrum of $Me_4Sn$.[37]

**Mössbauer spectroscopy.** The isomer shift, 1.27 mm $s^{-1}$, measured in the Mössbauer spectrum of dimethyltin anchored in zeolite Y, Fig. 3(a), indicates that the oxidation state of tin is IV. The large quadrupole splitting, 3.44 mm $s^{-1}$, speaks of the low symmetry surrounding the tin(IV) centres. The sample of pure dimethyltin in zeolite Y was prepared by titrating the protons while the sample was held at 150 °C, so that the reactivity was similar for the α- and β-protons. Thus every tin centre reacted with two protons immediately, and therefore about three tin centres, uniformly dimethyl species, were anchored in each α-cage. Quadrupole splittings of this size (3.44 mm $s^{-1}$) are usually indicative of low symmetry, such as trigonal bipyramidal stereochemistry, for compounds $(R_2SnX_2)_n$ or $(R_3SnX)_n$ where X is $F^-$, $Cl^-$, $Br^-$, $I^-$, or $O^{2-}$ donor.[31] Among alkyltin species with oxygen containing ligands, the size of the quadrupole splitting is dominated by the number and position of the alkyl ligands. For example, for dimethylated amino acid and Schiff base derivatives with octahedral structure and methyl groups *trans*, quadrupole splittings of up to 4.02 mm $s^{-1}$ have been reported[39] [$Me_2Sn$(acac)]. Distorting the octahedra such that the C—Sn—C bond angle is 160° reduces the quadrupole splitting to values such as 3.31 mm $s^{-1}$ (ref. 40) {$Me_2Sn$[*N*,*N*′-(2-hydroxytrimethylene)bis(salicylaldamine)]}, agreeing best with the splitting determined here. On going to more symmetric, trigonal bipyramidal structures with methyl groups both equatorial {$Me_2Sn$[*N*-(2-hydroxyphenyl)salicylaldimine]}, the quadrupole splitting drops to 3.04.[41] This suggests that the dimethyltin species, anchored over the three prominant oxygens of site II, probably has a structure intermediate between the latter two examples, a distorted 'octahedron' with one missing ligand, or a distorted trigonal bipyramid, with one methyl group equatorial and one axial.

It is also interesting to note in this data the possiblity of a Goldanskii–Karyagin effect, reflected in the difference in areas of the two peaks of the quadrupole doublet while similar peak widths (FWHH) are maintained.[42] This effect arises when there is an anisotropy in the Mössbauer recoil-free fraction, *i.e.*, the mean-square vibrational amplitude is not cubically symmetric. This is quite reasonable in a situation in which the recoiling species is effectively anchored to a surface site (*i.e.* the zeolite framework) such that the vibrational amplitude perpendicular to the 'wall' will likely be very different from that parallel to it. Further work would be required to prove such a point, but it remains an interesting possibility.

Fig. 3(b) shows the Mössbauer spectrum of $Sn_4S_6$-Y. The isomer shift of 1.25 mm $s^{-1}$ indicates that the oxidation state of tin is IV, as mentioned earlier, and the quadrupole splitting is 2.28 mm $s^{-1}$, considerably smaller than that of the precursor material. However, octahedral or tetrahedral symmetries have no intrinsic quadrupole splitting, and no alkyl groups are expected to contribute, as only sulfide and oxide ligands are expected. Therefore, an unsymmetric distribution of the different ligands about a tetrahedral or octahedral tin(IV) centre will probably describe the structure, consistent with the proposed adamantane structure. The isomer shift of the encapsulated cluster, 1.25 mm $s^{-1}$, agrees very closely with that measured for the methyl-capped cluster $Me_4Sn_4S_6$, 1.28 mm $s^{-1}$. However, the quadrupole splitting of the encapsulated cluster is considerably bigger than that of $Me_4Sn_4S_6$ (2.28 *vs.* 1.34 mm $s^{-1}$), probably because the latter has a more rigid symmetry, and alkyl groups more closely match the electronegativity of sulfide ligands than zeolite oxygens do. The observation of a single kind of tin(IV) Mössbauer site is consistent with the Rietveld PXRD structural conclusion, that the $Sn_4S_6^{4+}$ cluster is four-fold positionally disordered over the four site II oxygen six-ring positions in the α-cage of zeolite Y. Variable temperature Mössbauer studies (10–300 K) will be required to distinguish static from dynamic $Sn_4S_6^{4+}$ disorder in this system.

**Optical spectroscopy.** In Fig. 8 the optical reflectance data for four forms of tin sulfide are presented. Qualitatively, the spectrum of the encapsulated clusters, $Sn_4S_6$-Y, is considerably blue-shifted as compared to the bulk semiconductor berndtite, $SnS_2$. This is as expected for confinement of electrons within a quantum dot. However, it is quite similar to the spectrum of the molecular species, $(CH_3)_4Sn_4S_6$, indicating that the excitonic confinement regime was overshot. This species is within the very strong confinement size regime and is essentially molecular. Without good information about the effective masses of the electrons and holes in $SnS_2$ it is not possible to calculate the optimum cluster size for excitonic confinement, but it is clear that the size obtained was too small. An EHMO calculation for the isolated cluster was consistent with the qualitative molecular orbital diagram shown in Fig. 9, and indicated that the HOMO and LUMO were composed mainly of sulfur 3p and tin 5s and 5p orbitals, respectively, and give rise to a ligand-to-metal charge-transfer electronic transition as seen in the optical spectrum, Fig. 8.[43] In considering the possibility of intercluster coupling, the EHMO method was used to determine that clusters would need to have centre-to-

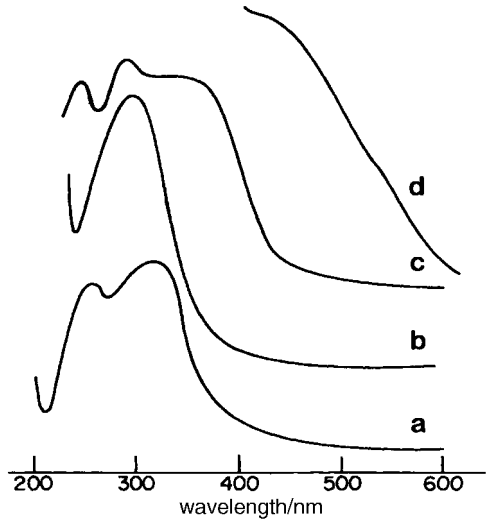


**Fig. 8** UV–VIS absorbance spectra of four forms of tin sulfide, (a) molecular $(CH_3)_4Sn_4S_6$, (b) zeolite encapsulated $Sn_4S_6$-Y, (c) $[(CH_3)_4N]_2Sn_3S_7$ denoted TMA-SnS-1, (d) bulk $SnS_2$, berndtite

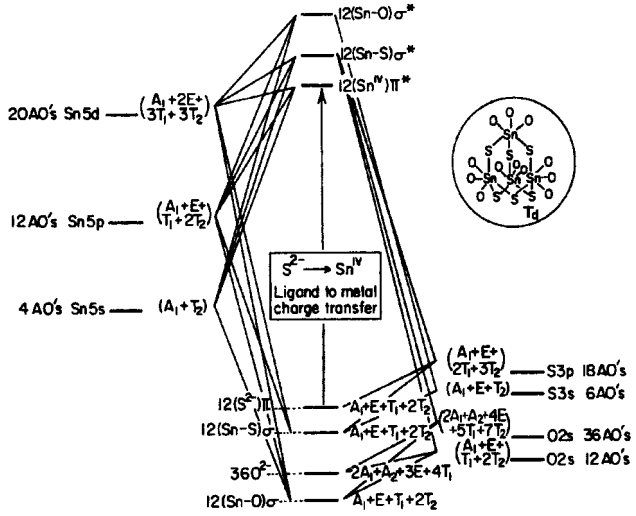


**Fig. 9** Extended Hückel molecular orbital, EHMO, energy diagram representing a zeolite-encapsulated $Sn_4S_6$ cluster

centre distances of less than 9 Å before any modification of their electronic structure was calculated. While the clusters were not expected to occupy the centres of the α-cages, which are 13 Å apart, there would nevertheless be an average intercluster distance of 13 Å over the whole material, which puts it outside this range for potential intercluster coupling. This of course does not account for any through-bond coupling, possible *via* the zeolite lattice. In comparison, in a microporous layered tin(IV) sulfide having the formula $R_2Sn_3S_7$ with $Sn_4S_3$, broken cube clusters linked by double sulfur bridges,[44] the clusters are less than 8 Å apart and are anticipated to be significantly coupled through the double sulfur bridges. The intermediate value of the absorption edge of $R_2Sn_3S_7$, Fig. 8, with respect to those of the bulk and molecular cluster forms of tin sulfide is noteworthy both in terms of connectivity arguments that have been put forward regarding the dimensionality of such materials,[45] and in the context of semiconductor quantum confinement and cluster-framework topological complements.[46]

As was discussed above, further growth of the tin sulfide clusters was possible and resulted in red-shifting of the absorption maximum, but the material was insufficiently homogeneous for good characterization. Nevertheless, Fig. 10 shows the results of cluster growth: a definite red-shift of the absorption edge on going from $Sn_4S_6$ clusters, (a), to clusters resulting from a second loading, (b), and from a third loading, (c). The red-shift is probably indicative of less confined charge carriers, due to an increase in the cluster size.[47] This supports the idea that the titration of regenerated protons and formation of more tin sulfide material in each α-cage does increase the nuclearity of the initial tin sulfide clusters.

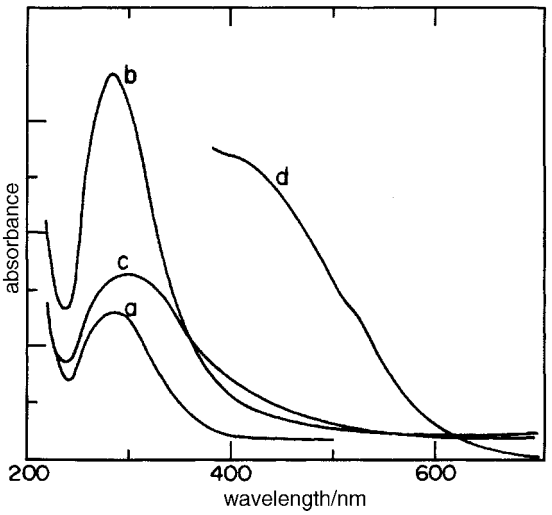


**Fig. 10** UV–VIS diffuse reflectance spectra of the products of (a) the first loading of $Sn_4S_6$ clusters in zeolite Y, (b) a second loading, titrating regenerated protons in order to add more tin sulfide material to each cluster, and (c) a third loading, increasing the cluster again, (d) bulk $SnS_2$

On a final note, one would expect that adamantanoid $Sn_4S_6$-Y might be grown from intrazeolite $Me_4Sn$ and $H_2S$ reagents, as it is well known that the solution phase reaction of $MeSnCl_3$ with $H_2S$ yields adamantane clusters, $Me_4Sn_4S_6$, with terminal methyl-capping groups. The four nucleophilic methyl groups of $Me_4Sn_4S_6$ are simply substituted in the zeolite encapsulated analogue by charge-balancing framework oxygens to give $(ZO)_4Sn_4S_6$ according to the zeolate model of bonding.[23]

## Conclusions

The application of size-limiting intrazeolitic MOCVD techniques has been demonstrated to be a method of choice for the synthesis of arrays of zeolite encapsulated IV–VI semiconductor clusters. Step-wise, molecule-by-molecule control over the intrazeolite reaction processes is possible by employing non-intrusive, quantitative, *in situ* methods of observing them, as shown in this work. Charge-balancing tin sulfide clusters of average $Sn_4S_6^{4+}$ stoichiometry have been synthesised in the α-cages of zeolite Y, possibly with an adamantanoid geometry. It is expected that the methodologies presented in this paper will be generally applicable to other semiconductor clusters within other media in syntheses that are equally controllable. It should be noted that, at the time this work was done, clusters in zeolites had an upper limit of 13 Å imposed by the restricted choice of large-cage zeolites. Since then the world of size-controlled large-aperture mesoporous silicas, beginning with MCM-41,[48] has opened up, and ordered channels of 20–100 Å are available as hosts for this type of CVD topotaxy.[49]

The authors are indebted to Dr Robert Broach and Dr Robert L. Bedard for valuable discussion regarding the Rietveld analysis. The PXRD measurements were carried out at the National Synchrotron Light Source, Brookhaven National Laboratories which is supported by the US Department of Energy, Division of Materials Sciences and the Division of

Chemical Sciences. We acknowledge the Natural Sciences and Engineering Research Council of Canada (NSERC) as well as the Canadian Space Agency (CSA) and UOP for financial support of this endeavour. In addition, C.B. thanks NSERC and the University of Toronto for financial support during her graduate work.

## References


1 P. Day, *Chem. Br*., 1996, July, 29.
2 M. A. Reed, J. N. Randall, R. J. Aggarwal, R. J. Metyi, T. M. Moore and A. E. Wetsel, *Phys. Rev. Lett*., 1988, **60**, 535.
3 R. F. Pease, in *Nanostructures and Mesoscopic Systems*, ed. W. P. Kirk and M. A. Reed, Academic Press, Toronto, 1992.
4 F. R. Waugh, M. J. Berry, D. J. Mar, R. M. Westervelt, K. L. Campman and A. C. Gossard, *Phys. Rev. Lett*., 1995, **75**, 705.
5 K. Kash, D. D. Mahoney, B. P. Van der Gaag, A. S. Gozdz, J. P. Harbinson and L. T. Florenz, *J. Vac. Sci. Technol. B*, 1992, **10**, 2030.
6 G. A. Ozin, *Adv. Mater*., 1992, **4**, 612.
7 N. Herron, Y. Wang and H. Eckert, *J. Am. Chem. Soc*., 1990, **112**, 1322.
8 M. A. Matchett, A. M. Viano, S. L. Adolphi, R. D. Stoddard, W. E. Buhro, M. S. Conradi and P. C. Gibbons, *Chem. Mater*., 1992, **4**, 508.
9 M. L. Steigerwald, A. P. Alivisatos, J. M. Gibson, T. D. Harris, R. Korton, A. J. Muller, A. M. Thayer, T. M. Duncan, D. C. Douglass and L. E. Brus, *J. Am. Chem. Soc*., 1988, **110**, 3046; Y-M. Tricot and J. H. Fendler, *J. Phys. Chem*., 1986, **90**, 3369; X. K. Zhao, S. Baral, R. Rolandi and J. H. Fendler, *J. Am. Chem. Soc*., 1988, **110**, 1012; J. H. Fendler and F. C. Meldrum, *Adv. Mater*., 1995, **7**, 607.
10 Y. Wang, A. Suna, W. Mahler and R. Kasouuwski, *J. Chem. Phys*., 1987, **87**, 7315; E. S. Smotkin, R. M. Brown, Jr., L. K. Rabenberg, K. Salomon, A. J. Bard, A. M. A. Campion, M. A. Fox, T. Mallouk, S. E. Webber and J. M. White, *J. Phys. Chem*., 1990, **94**, 7543.
11 F. Yan and J. M. Parker, *J. Non-Cryst. Solids*, 1989, **112**, 277; R. D. Stramel, T. Nakamura and J. K. Thomas, *J. Chem. Soc., Faraday Trans*., 1988, **84**, 1287.
12 N. Herron, Y. Wang, M. M. Eddy, G. D. Stucky, D. E. Cox, K. Moller and T. Bein, *J. Am. Chem. Soc*., 1989, **111**, 530; J. E. MacDougall, H. Eckert, G. D. Stucky, N. Herron, Y. Wang, K. Moller and T. Bein, *J. Am. Chem. Soc*., 1989, **111**, 8006.
13 C. B. Murray, C. R. Kagan and M. G. Bawendi, *Science*, 1995, **270**, 1335.
14 A. P. Alivisatos, *Science*, 1996, **271**, 933.
15 P. M. Petroff and G. Madeiros-Ribeiro, *MRS Bull*., 1996, **21**, 50.
16 C. A. Fyfe, J. M. Thomas, J. Klinowski and G. C. Gobbi, *Angew. Chem*., 1983, **22**, 259.
17 G. A. Ozin and J. Godber, *J. Phys. Chem*., 1988, **92**, 4980; 2841.
18 R. W. Frei and J. D. MacNeil, *Diffuse Reflectance Spectroscopy in Environmental Problem Solving*, CRC Press, Cleveland, OH, 1973.
19 A. C. Larson and R. B. Von Dreele, *Generalized Structure Analysis System*, LAUR 86-748, Los Alamos National Laboratory, Los Alamos, NM 87545, USA.
20 ICONCL software: OS/2 Version, MS-Fortran 5.0, 30 November 1989, Modified ICON8 from QCPE 344, Calzaferri Group, Institute for Inorganic Chemistry, University of Bern, Switzerland.
21 J. H. Ammeter, H.-B. Burgi, J. C. Thibeault and R. Hoffman, *J. Am. Chem. Soc*., 1978, **100**, 3686.
22 G. Clazaferri, L. Forss and I. Kamber, *J. Phys. Chem*., 1989, **93**, 5366.
23 G. A. Ozin, C. L. Bowes and M. R. Steele, *Mater. Res. Soc. Symp. Proc*., 1992, **277**, 105.
24 G. A. Ozin and S. Ozkar, *Chem. Mater*., 1992, **4**, 51; G. A. Ozin, A. Kuperman and A. Stein, *Angew. Chem., Int. Ed. Engl*., 1989, **101**, 373; G. A. Ozin, S. Ozkar and R. A. Prokopowicz, *Acc. Chem. Res*., 1992, **25**, 553; G. A. Ozin, *Adv. Mater*., 1992, **4**, 612; G. A. Ozin, *Adv. Mater*, 1992, **4**, 11.
25 D. H. Olsen and E. Dempsey, *J. Catal*., 1969, **13**, 221.
26 J. W. Ward, *J. Catal*., 1967, **9**, 396.
27 G. A. Ozin, S. Ozkar and L. McMurray, *J. Phys. Chem*., 1990, **94**, 8297.
28 T. Yamazaki, I. Watanuki, S. Ozawa and Y. Ogino, *Langmuir*, 1988, **4**, 433.
29 G. A. Ozin, S. Ozkar and L. McMurray, *J. Phys. Chem*., 1990, **94**, 8289.
30 L. Quanzi, A. Ruiming and X. Zhiyuan, in *New Developments in Zeolite Science and Technology*, ed. Y. Murakami, A. Iijima and J. W. Ward, Elsevier, New York, 1986, p. 487; J. J. Lunsford, P. N. Tutunjian, P. Chu, E. B. Yeh and D. J. Zalewski, *J. Chem. Phys*., 1989, **93**, 2590 and references therein.
31 R. V. Parish, in *Mössbauer Spectroscopy Applied to Inorganic Chemistry*, ed. G. J. Long, Plenum Press, N.Y., 1984, vol. 1, ch. 16.
32 G. A. Ozin, S. Ozkar and G. D. Stucky, *J. Phys. Chem*., 1990, **94**, 7562.
33 J. Howard and Z. A. Kadir, *Spectrochim. Acta*, *Part A*, 1985, **41**, 825 and references therein.
34 A. K. Cheetham and A. J. Skarnulis, *Anal. Chem*., 1981, **53**, 1060.
35 B. Krebs, *Angew. Chem., Int. Ed. Engl*., 1983, **22**, 113.
36 X. Hu and W. Depmeier, *Z. Kristallogr*., 1992, **201**, 99.
37 W. F. Edgell and C. H. Ward, *J. Am. Chem. Soc*., 1955, **77**, 6486.
38 P. R. Bunker, *Molecular Symmetry and Spectroscopy*, Academic Press, New York, 1977; R. L. Flurry, *Symmetry Groups, Theory and Chemical Applications*, Prentice Hall, NJ, 1980.
39 T. K. Sham and G. M. Bancroft, *Inorg. Chem*., 1975, **14**, 2281.
40 J. N. R. Ruddick and J. R. Sams, *J. Organomet. Chem*., 1973, **60**, 233.
41 J. N. R. Ruddick and J. R. Sams, *J. Chem. Soc*., *Dalton Trans*., 1974, 470.
42 V. I. Goldanskii, G. M. Gorodinskii, W. V. Karyagin, L. A. Korytko, L. M. Krizhanski, E. F. Makarov, I. P. Suzdalev and V. V. Khrapov, *Dokl. Akad. Nauk SSSR*, 1962, **147**, 127; S. V. Karyagin, *Dokl. Akad. Nauk SSSR*, 1963, **148**, 1102.
43 C. L. Bowes, MSc Thesis, University of Toronto, 1991.
44 C. L. Bowes, S. Petrov, G. Vovk, D. Young, G. A. Ozin and R. L. Bedard, *J. Mater. Chem*., 1998, **8**, 711.
45 E. A. Axtell III, J-H. Liao, Z. Pikramenou, Y. Park and M. G. Kanatzidis, *J. Am. Chem. Soc*., 1993, **115**, 12191; E. A. Axtell III, J-H. Liao, Z. Pikramenou and M. G. Kanatzidis, *Chem. Eur. J*., 1996, **2**, 656.
46 C. L. Bowes and G. A. Ozin, *Mater. Res. Soc. Symp. Proc*., 1992, **286**, 93.
47 L. E. Brus, *J. Chem. Phys*., 1984, **80**, 4403; Y. Kayanuma, *Phys. Rev. B*, 1988, **38**, 9797.
48 C. T. Kresge, M. E. Leonowicz, W. J. Roth, J. C. Vartuli and J. S. Beck, *Nature*, 1992, **359**, 710.
49 C. L. Bowes, A. Malek, G. A. Ozin, *Chem. Vap. Deposit*. (*Adv. Mater*.), 1996, **2**, 97.


*Paper* 7/08093J; *Received* 11*th November*, 1997